The effects of interparticle interactions and particle size on reversible shear thickening: Hard-sphere colloidal dispersions

Brent J. Maranzano and Norman J. Wagner[a)]

Center for Molecular and Engineering Thermodynamics, Department of Chemical Engineering, University of Delaware, Newark, Delaware 19716

(Received 2 February 2001; final revision received 15 June 2001)

Synopsis

A comparison between the effects of two colloidal stabilizing methods (electrostatic versus Brownian) on the reversible shear thickening transition in concentrated colloidal suspensions is explored. Five suspensions of monodisperse silica are synthesized via the Stöber synthesis and dispersed in an index matched organic solvent to minimize van der Waals interactions. The residual surface charge is neutralized with nitric acid ($c_{HNO_3} \approx 0.1$ M) resulting in a near hard-sphere interaction that is confirmed by small angle neutron scattering measurements across a range of volume fractions. Rheological measurements demonstrate the effects of neutralization on the low shear and high shear rheology, which show that the onset of shear thickening moves to lower applied shear stresses and scales inversely with particle size cubed, in agreement with theory. Quantitative comparisons of both the low shear viscosity and the critical stress for shear thickening to predictions for hard spheres and literature data demonstrate the extreme sensitivity of high shear rheology to the surface properties in concentrated suspensions. © *2001 The Society of Rheology.*
[DOI: 10.1122/1.1392295]

I. INTRODUCTION

The hard-sphere potential is a favored base system for studies involving the thermodynamics, microstructure, dynamics, and rheology of colloidal and molecular fluids because it can be presented by a single parameter, the hard sphere radius. Beginning with Einstein's analysis (1906) on the viscosity of infinitely dilute suspensions of rigid spheres, many investigations have attempted to predict the rheology and diffusion of hard-sphere colloidal dispersions from first principles. Much of the effort has focused on extending theoretical models for dilute dispersions to concentrated dispersions of Brownian hard spheres [Frankel and Acrivos (1967), Batchelor (1970), Batchelor (1977), Batchelor and Green (1972), Jeffrey and Acrivos (1976), Russel and Gast (1986), Wagner and Russel (1989), Lionberger and Russel (1997), Brady (1993), Brady and Morris (1997)]. Commensurate with these theoretical developments, experimentalists have worked toward developing real colloidal dispersions that approximate hard spheres [Krieger and Dougherty (1959), de Kruif *et al.* (1985), van der Werff and de Kruif (1989), van der Werff *et al.* (1989), Segre and Pusey (1997), Wagner and Russel (1990), Frith *et al.* (1996), Meeker *et al.* (1997)]. Computational techniques that include many body hydrodynamic interactions have also been developed to enable direct numerical calculation of

[a)]Author to whom correspondence should be addressed. Electronic mail: wagner@che.udel.edu

hard-sphere colloidal behavior [Brady and Bossis (1988), Foss and Brady (2000), Catherall *et al.* (2000), Melrose and Ball (1995), Melrose and Ball (1997)].

Rigorous testing of these theories and simulations requires extensive experimental data for the microstructure and rheology of model hard-sphere dispersions. For this purpose, a variety of synthesis strategies have been pursued to achieve model hard-sphere suspensions, which include suspensions of silica spheres with octadecyl alcohol grafted coatings dispersed in cyclohexane and other organic solvents [Wagner *et al.* (1988), van der Werff and de Kruif (1989), de Kruif *et al.* (1985), Rueb and Zukoski (1998)]. Some investigators have employed silica coated with 3-(trimethoxysilyl) propyl methacrylate (TPM) dispersed in index-matching tetrahydrofurfuryl alcohol (THFFA) [Wagner and Russel (1990), Bender and Wagner (1995), Maranzano *et al.* (2000)]. While others have explored polymethylmetacrylate (PMMA) particles stabilized by a chemically grafted, solvated layer of poly(12-hydroxystearic acid) (PHSA) suspended in decalin, tetralin, and other mixed solvents [Kaffashi *et al.* (1997), Meeker *et al.* (1997), Phan *et al.* (1996), Frith *et al.* (1996)]. Of particular interest here is the use of Stöber silica dispersions coated with TPM and dispersed in THFFA, which have been used previously to study the shear thickening rheology of concentrated hard-sphere dispersions [Bender and Wagner (1996), OBrien and Mackay (2000), Maranzano and Wagner (2001)].

At high concentrations close to the maximum packing fraction, the surface-to-surface separation for colloidal spheres becomes on the order of nanometers or less, such that minor deviations from mathematical smoothness have enormous consequences on the rheology. Surface asperities, roughness, chemical inhomogeneity, dangling ends of polymers on polymer colloids, grafted polymer heterogeneities, polydispersity, particle shape, and residual surface charge create noticeable deviations from mathematical hard spheres when particles are either in contact or nearly touching. Deviations are particularly pronounced at high shear rates where shear thickening is predicted to occur. True, mathematical hard spheres are expected to ''jam'' and solidify under very strong flow at high concentrations [Farr *et al.* (1997)], whereas even the slightest deviations from the mathematically hard-sphere potential lead to systems that exhibit a weak shear thickening where the viscosity increases logarithmically with shear rate [Bossis and Brady (1989), Brady and Morris (1997), Foss and Brady (2000), Dratler and Schowater (1996), Melrose and Ball (1995), Wilson and Davis (2000)]. As has been recently illustrated by the approximate Stokesian dynamics calculations of Melrose [Melrose *et al.* (1996)], the presence of a conservative force due to adsorbed or grafted polymer has a dramatic influence on the shear thickening rheology. The effect of an added conservative force is to increase the stress required for shear thickening and prevent the ''jamming transition,'' whereas modification of the lubrication hydrodynamics due to solvent penetration into the polymer brush leads to dramatic enhancement of the viscosity in the shear thickening state. To date there have been no definite experimental verifications of these predictions.

Here, we explore the dependence of the shear thickening rheology and the critical stress for the onset of shear thickening on dispersion concentration and particle size for nearly monodisperse, near hard-sphere suspensions. The suspensions are derived by removing the residual surface charge from weakly electrostatic stabilized, near hard-sphere dispersions that have been extensively studied in a previous publication [Maranzano and Wagner (2001)]. Comparisons of neutron scattering and electrophoretic mobility measurements before and after the acidification verify the hard-sphere interactions of the ''charge-neutralized'' dispersions. Rheology measurements demonstrate the accompanying change in the low and high shear viscosities, and are used to test model predictions for hard spheres.

II. METHODOLOGY

A detailed discussion of the particle synthesis and dispersion characterization is presented in [Maranzano and Wagner (2001)], so only a brief description is presented here. A set of chemically analogous dispersions are prepared via the Stöber synthesis [Philipse and Vrij (1988), van Blaaderen and Vrij (1993)], where seeded growth is used to vary particle size. The reaction is terminated by adding a stoichiometric quantity of a silane coupling agent, TPM, which eliminates most ($>$ 98%), but not all, of the surface silanol groups [Maranzano *et al.* (2000), Philipse and Vrij (1988)]. The particles are resuspended in an index matched organic solvent, tetrahydrofurfuryl alcohol (reagent grade Aldrich $\rho = 1.054$ g/cm^3, $n_D^{20} = 1.4512$, $\mu = 5.44$ cP), by repetitive centrifugation and suspending. The matching of the refractive indices minimizes the attractive dispersion forces, such that the resulting suspensions are weakly charge stabilized and can be considered near hard-sphere dispersions.

In this work, the remaining unreacted silanol groups are reassociated by adding aqueous nitric acid (Fisher Scientific, normality = 15.8) as suggested by Philipse [Philipse and Vrij (1988)]. Measurements on dilute dispersions in THFFA using a Brookhaven Zeta-PALS instrument are used to determine the necessary nitric acid concentration, which ranges from a solvent molarity of 0.066–0.15 M HNO_3 and varies systematically with the measured zeta potential of the original particles.

Characterization of the dispersions is performed through a variety of experimental techniques. The particle size distributions are determined and verified through transmission electron microscopy (TEM), dynamic light scattering (DLS), and, when applicable, small angle neutron scattering (SANS) measurements, which also demonstrates that the particles are spherical. The particle densities are measured from solution densitometry and dilution viscometry experiments. Solution densitometry measures the SiO_2 density, whereas dilution viscometry estimates the density based on the hydrodynamic size of the particles. Volume fractions are calculated from drying experiments, where the densities from solution densitometry are used to convert the weight fractions to volume fractions. Further details of the particle characterization are discussed elsewhere [Maranzano and Wagner (2001)].

Small angle neutron scattering measurements performed on the charge-neutralized dispersions are compared with measurements on the original dispersions to demonstrate the elimination of electrostatic interactions. The scattering data is obtained at the National Institute of Standards and Technology in Gaithersburg, MD on a 30 m SANS instrument using thermal neutrons with a 6 Å wavelength and 14.7% half-width triangular dispersity at a sample to detector distance of 12 m, using 1 mm sandwich cells. The measured intensities are reduced and put on an absolute scale following standard procedures.

The equation relating the measured scattering intensity $I(q)$ to the suspension microstructure is given in the following equation:

$$I(q) = \phi V_p \Delta\rho^2 P(q) S(q). \tag{1}$$

In this equation, ϕ is the volume fraction, V_p is the volume of a particle, $\Delta\rho$ is the scattering length density difference between the solvent (THFFA) and the particle, $P(q)$ is the form factor, and $S(q)$ is the structure factor. For polydisperse suspensions, the form factor and structure factor corresponding to the appropriate distribution is to be calculated for use in Eq. (1) [Wagner *et al.* (1991)]. Maranzano and co-workers (2000) have demonstrated that the residual silanol groups that remain after coating the silica dispersions with the silane coupling agent (TPM), provide a weak, but measurable electrostatic interaction between the particles. They found that SANS spectra of these concentrated

dispersions cannot be fit with hard sphere models, but are well described by a Yukawa model that includes the electrostatic interactions. In the analysis here, the form factor scattering is calculated for a Schulz distribution of homogeneous spheres, with a polydispersity determined from TEM measurements, and a particle radius adjusted to optimize the fit. The structure factor is calculated using the Percus–Yevick integral equation for polydisperse hard spheres following a Schulz distribution [Griffith *et al.* (1987)], where the volume fraction is calculated from the measured solids weight fraction by using the particle density derived from solution densitometry.

The rheological measurements are conducted on a Bohlin controlled stress rheometer. The rheometer has a torque range of 0.001–10 mN m with a torque resolution of 0.0002 mN m and an angular deflection resolution of 1.6 μrad. The data reported here are produced with: 20 mm 4°, and 20 mm 1° cone and plates. A study of these dispersions without the addition of nitric acid [Maranzano and Wagner (2001)] employed additional cone and plates and couette geometries, as well as an RMS 800 strain rate controlled rheometer, to verify that the dispersion rheology is not dependent on the tooling or geometry.

Previous investigations on concentrated dispersions have shown that shear history has a profound impact on experimental data [Chow and Zukoski (1995)]. Therefore, the following protocol is strictly adhered to for all measurements.

(1) A 3 min stress ramp from 0.1 to 4700 Pa to remove shear history effects.
(2) A 2 min creep experiment at a shear stress corresponding to a shear rate of 1 s^{-1} followed by 30 s recovery.
(3) A stress sweep from 0.5 to 4700 Pa obtaining 20 logarithmically spaced points. The sample was allowed to equilibrate for 10 s before each stress measurement followed by averaging the viscosity response for 20 s. Note: The maximum stress for dilute suspensions was dictated by a maximum achievable shear rate before the sample fractured.
(4) A stress sweep from 0.06 to 10 Pa with 1 min equilibration and 2 min averaging.
(5) A stress sweep near the critical shear stress collecting 30 points with 10 s equilibration and 20 s averaging.
(6) A frequency sweep from 0.1 to 100 Hz at 1% strain.
(7) A 2 min creep experiment at a shear stress corresponding to a shear rate of 1 s^{-1} followed by 30 s recovery.

Data sets that exhibit substantial differences between the first and last creep experiments, which are thought to be due to drying effects, are rejected and a new sample is tested.

The zero shear viscosity data are used to assess the effective volume fraction changes between the charge-neutralized and original dispersions. The apparent zero shear viscosity of the unneutralized dispersions are determined by fitting the low shear viscosity data to a constitutive relation for a power-law shear thinning fluid with a yield stress [Maranzano and Wagner (2001)]. Contrarily, rheology measurements on hard sphere suspensions exhibit a low-shear Newtonian plateau, and thus the zero shear viscosities of the charge-neutralized dispersions are calculated by averaging the measured low shear viscosities. The zero shear viscosity dta is fit to a Krieger–Dougherty (1959) relation, $\eta_r = (1 - \phi/\phi_{\max})^{-2.5\phi_{\max}}$, using the maximum packing fraction, $\phi_{\max}$, as an adjustable parameter. The effective volume fraction is then estimated by comparing the maximum packing fraction of the suspensions to the packing fraction where the viscosity diverges for hard spheres ($\phi = 0.58$).

The transition to the shear thickening regime for very small particle sizes can occur at high shear rates, where the onset of secondary flows is a concern. We model the secondary flow effects for each tooling using rheological data from Newtonian silicone oils as discussed in detail by Maranzano and Wagner (2001). The critical stress values at the onset of shear thickening are extracted from fitting a double log plot of the flow curves with a quadratic polynomial. The minimum of the fit gives the critical stress, τ_c, and critical viscosity, η_c.

III. SCALING THEORY FOR SHEAR THICKENING

The onset of reversible shear thickening in colloidal dispersions is predicted to occur when the compressive hydrodynamic force between two particles in the suspension becomes larger than the total repulsive force between particles, leading to the formation of a hydroclustered state. The hydroclustered state manifests itself as strong, hydrodynamic contributions to the viscosity that can, at high volume fractions, lead to slip and sample fracture [Bossis and Brady (1989), D'Haene *et al.* (1993), Bender and Wagner (1996), OBrien and Mackay (2000)]. Based on this mechanism, a simple two-particle model has been proposed to predict the onset of shear thickening for Brownian hard spheres suspensions [Bender and Wagner (1996)]. A dimensionless shear stress for the onset of shear thickening, denoted as the ''critical'' shear stress, is defined by the ratio of the lubrication hydrodynamic force, with a mean-field correction for the suspension viscosity, to the Brownian force [Eq. (2)]:

$$\tau_{cr}^{Br} = \frac{F_{\text{hydrodynamic}}(\tau_c)}{F_{\text{Brownian}}} = \frac{3\pi\mu a^3\dot{\gamma}_c/2h}{-k_BT\partial \ln g(r)/\partial r|_{r=2a+h}}\left(\frac{\eta_c}{\mu}\right)$$
$$= \frac{3\pi\tau_c a^3/2h}{-k_BT\partial \ln g(r)/\partial r|_{r=2a+h}}. \tag{2}$$

Here, a is the particle radius, h is the separation distance between particle surfaces, which is approximated by $h/2a = (\phi/0.71)^{-1/3}-1$, $g(r)$ is the equilibrium pair distribution function as a function of center to center separation distance (r), and the quantities, τ_c, $\dot{\gamma}_c$, and η_c are the shear stress, shear rate, and viscosity, respectively, at the onset of reversible shear thickening.

As reported by Maranzano and Wagner [Maranzano and Wagner (2001)] for the unneutralized dispersions (i.e., weakly charge stabilized), a similar scaling, where electrostatic repulsion replaces the Brownian repulsion, partially reduces the measured critical stress for shear thickening across a series of dispersions of varying particle size and concentration. Furthermore, it has been demonstrated that a quantitative prediction for the onset of shear thickening is possible with a model first proposed by Melrose and Ball [Melrose and Ball (2000)]. This model includes a comparison of time required for the conservative forces to separate a particle pair relative to the time scale of the flow, and hypothesizes they are equal at the onset of shear thickening. When modified with a mean-field correction to account for the many-body hydrodynamic interactions in the concentrated dispersion, this balance results in the following reduced critical stress for shear thickening of a hard-sphere colloidal dispersion

$$\tau_{cr}^{M} = \frac{3\pi\tau_c a^3/2h_m}{-k_BT\partial^2 \ln g(r)/\partial r^2|_{r=2a+h_m}}. \tag{3}$$

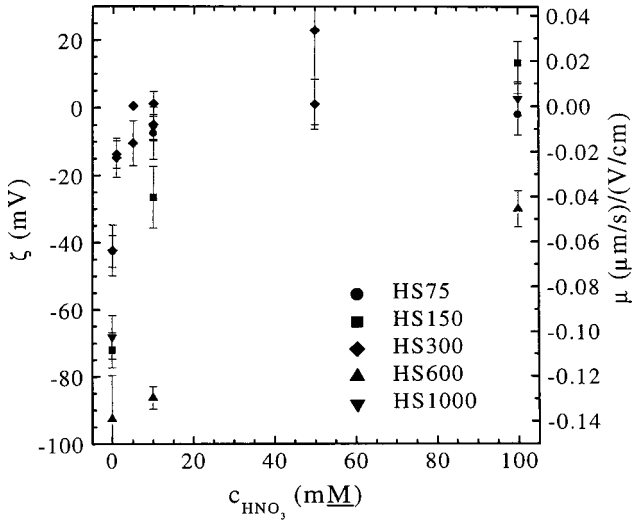

FIG. 1. Zeta potentials and electrophoretic mobilities as a function of the concentration of nitric acid for the various dispersions studied in this investigation.

In the earlier equation, the characteristic surface-to-surface separation distance, h_m, is obtained from a balance of the applied shear stress and the repulsive Brownian force as

$$\tau_c 4a^2 = -k_B T \left.\frac{\partial \ln g(r)}{\partial r}\right|_{r = 2a+h_m}. \tag{4}$$

A derivation of this equation can be found in Melrose and Ball (2000), and Maranzano and Wagner (2001), where the Brownian force is used as the repulsive force. This two-particle model provides an estimate of the shear stress required to generate the incipient hydroclustered microstructure from the properties of the dispersion.

IV. RESULTS

First, it is important to establish the degree to which acidification of the coated dispersions in index-matching solvent leads to hard-sphere like behavior. Figure 1 illustrates the change in zeta potential and electrophoretic mobility with decreasing *p*H due to addition of nitric acid.

The Brookhaven Zeta-PALS can accurately resolve particle mobilities as low as ~ 0.01 (μm/s)/(V/cm), which translates to zeta potentials of ~ 7 mV for the solutions considered here. Figure 1 demonstrates that the electrophoretic mobility of the HS300 dispersion becomes smaller than the instrument limits at 5 mM HNO_3, and is less than measurement error for all but the highly charged dispersions (HS150 and HS600) at 10 mM HNO_3. From these measurements we estimate the necessary concentrations of HNO_3 to neutralize the residual surface charges, and find that the concentrations range from 0.066 to 0.15 M as summarized in Table I. This table also summarizes the particle characterization, which includes radius (a), aspect ratio (a/b), rotational diffusivity (Θ_0), density (ρ), zeta potential (ζ), Huggins coefficient (κ_H), relative double layer thickness (ka), maximum packing fraction ($\phi_{\max}$), and calculated deviation in radius based on $\phi_{\max} = 0.58(\Delta r)$.

TABLE I. Particle characterization summary.

	HS75	HS150	HS300	HS600	HS1000
a_{TEM} (nm)	75±7.3	167.3±14.8	302.0±26.2	608.6±80.8	656.4±64.3
a_{DLS} (nm)	88.8±0.8	177.8±4.1	330.7±19.5	633.1±114.4	845.5±184.8
a_{SANS} (nm)	71.0±7.0	162.0±14.3	318.0±16.7		
a/b	1.07±0.06	1.04±0.03	1.03±0.02	1.04±0.1	1.03±0.04
Θ_0 (s^{-1})	−100.5±1.0	−2.94±7.6	2.92±14.1	60.4±5.9	8.2±68.6
ρ_{SiO_2} (g/cm^3)	1.70±0.01	1.90±0.01	1.82±0.01	1.85±0.01	1.76±0.04
$\rho_{particle}$ (g/cm^3)	1.45±0.02	2.16±0.02	1.82±0.08	1.87±0.13	1.77±0.10
ζ (mV)	−42.6±4.7	−72.1±5.3	−42.3±7.5	−92.7±13.1	−68.2±6.5
κ_H	3.78±1.24	2.28±1.24	0.61±0.93	1.18±2.46	3.6±1.24
$\kappa a(\phi = 0.5)$	13.2±1.3	28.5±2.5	4.17±3.62	87.1±11.6	89.9±8.8
ϕ_{max}	0.38	0.38	0.46	0.52	0.51
c_{HNO_3}(mM)	66	110	100	150	110
ϕ_{max}	0.48	0.45	0.54	0.58	0.52
Δr (nm)	2.5	7.9	3.5	0	12

Philipse and Vrij (1998) reported the elimination of electrophoretic mobilities of similar particles suspended in ethanol and ethanol-toluene mixtures with the addition of 0.001 M HNO_3. The discrepancy between our measurements and Philipse and Vrij may be due to the difference in the dissociation constant of the surface silanol groups in the two different solvents, or the enhanced resolution of the zeta-PALS instrument used in this study. For reference, bare silica dispersions dispersed in water exhibit an isoelectric point at $p\mathrm{H} \approx 2$ [Iler (1955)], which corresponds to 0.01 M HNO_3 in water. One consequence of adding aqueous nitric acid is the inclusion of water accompanying the nitric acid. As a result of adding aqueous nitric acid, we estimate that the dispersion solvent contains approximately 0.2 M water. Electrorheological investigations of silica in organic solvents have demonstrated the consequences of residual water in enhancing surface silanol dissociation [Gast and Zukoski (1989)]. Indeed, the zeta potential of our dispersions is observed to progress through the isoelectric point and change sign with the addition of water ($\sim$ 2 M) for a given acid molarity of 0.05 M. For this reason, the composition of the solvent, with respect to water, is held constant.

Figure 2 displays the SANS spectra measured on the charge-neutralized HS75 dispersions. The parameters used in the theoretical fits are given in Table II. The predicted scattering spectra for polydisperse hard spheres ($a = 35.5$ nm, $\sigma_p = 9.8\%$) are seen to fit the data very well across the concentration series, which conforms the hard-sphere interactions. Note that in the theoretical calculation of the structure factor, the particle size, polydispersity, and volume fraction are independently determined. The scattering length density difference determined from the linear dependence of the forward scattering intensity with particle concentration yields $|\Delta\rho| = 3.0\times10^{10}$ cm^{-2}, which is in reasonable agreement with the previous reported result of 2.8×10^{10} cm^{-2} [Maranzano *et al.* (2000)]. We also note that SANS data collected during shear in both tangential and radial geometries confirm that the suspensions remain liquid-like and that no order-disorder transition [Laun *et al.* (1992), Hoffmann (1972)] accompanies the reversible shear thickening transition [Maranzano (2001)].

The effect of added acid is evident in Fig. 3, which compares the scattering between the original and charge-neutralized dispersions at two similar volume fractions. Both scattering curves for the charge-neutralized dispersions show much less structure (smaller primary peaks) than the corresponding scattering curves from the original dispersions.

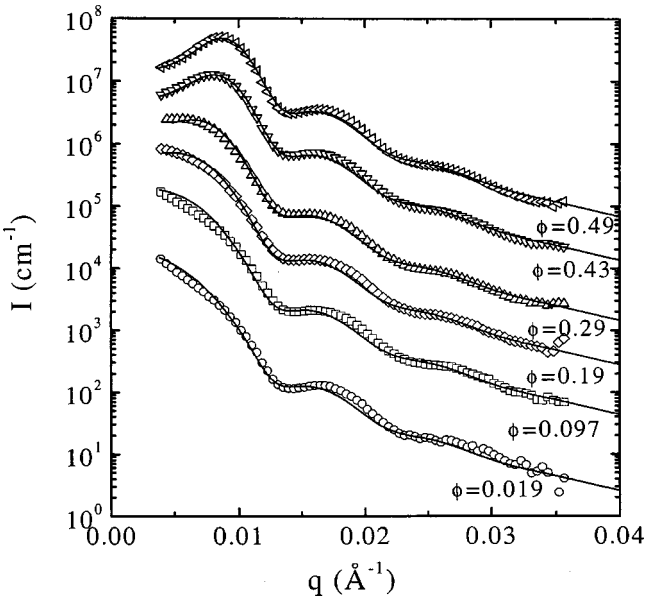

FIG. 2. SANS spectra for the HS75 dispersion with 0.066 M HNO_3 at several concentrations (symbols) compared to the calculated scattering intensities for polydisperse suspensions of hard spheres (a = 35.5 nm, σ_p = 9.8%) (lines). The data have been offset for clarity.

This is particularly evident around a volume fraction of 0.3, where the weakly charged dispersion shows a substantial first peak. However, the nearest neighbor correlation peak is suppressed for the dispersion with 0.066 M HNO_3. The decrease in the amount of structure in the scattering upon addition of HNO_3 is due to the neutralization of the electrostatic interactions that are present in the weakly charged dispersions.

From the electrophoretic mobility and SANS measurements we conclude that these dispersions are described by a hard-sphere potential to within state-of-the-art measurement accuracy. Note, however, that these silica dispersions do not exhibit the hard-sphere fluid-crystal transition evident for PMMA dispersions [Ackerson and Pusey (1988), Phan *et al.* (1996)]. The reason for the loss of the weak first order phase transitions in the silica dispersions may be related to their density mismatch.

The sensitivity of the zero shear viscosity to interparticle interactions also provides evidence for the near hard sphere behavior of the charge-neutralized dispersions. Figure 4 displays the zero shear viscosities of the original and charge-neutralized dispersions

TABLE II. Dispersion parameters used in SANS fits in Fig. 2.

ϕ	a (nm)	σ_a (nm)	$I(0)$ (cm^{-1})
0.019	35.5	3.5	2200
0.097	35.5	3.5	19 000
0.19	35.5	3.5	26 000
0.29	35.5	3.5	46 000
0.43	35.5	3.5	76 000
0.49	35.5	3.5	48 000

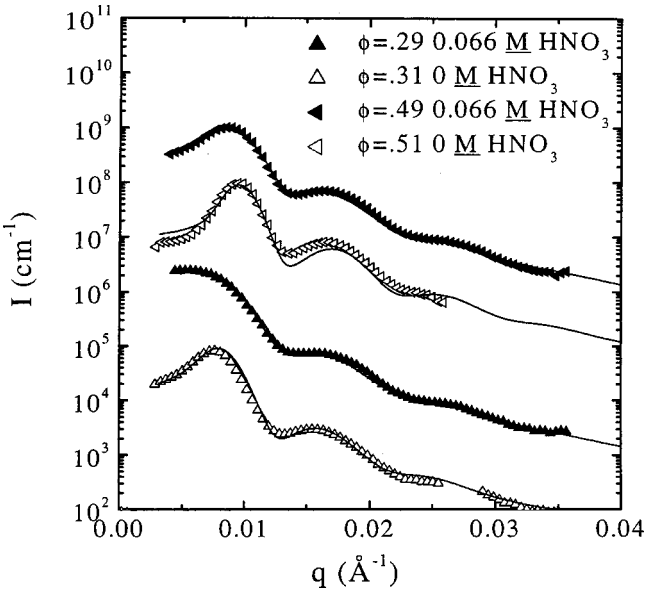

FIG. 3. SANS data comparison between the HS75 dispersion with 0.066 M HNO_3 (filled symbols) compared to the same dispersions with 0 M HNO_3 (open symbols). The data have been offset for clarity.

plotted against volume fraction normalized by the maximum packing volume fraction for each dispersion, which are listed in Table I. The data follow the Krieger and Dougherty (1959) relation $\eta_r = (1-\phi/\phi_{\max})^{-2.5\phi_{\max}}$, with $\phi_{\max} = 0.58$, as expected for near hard spheres.

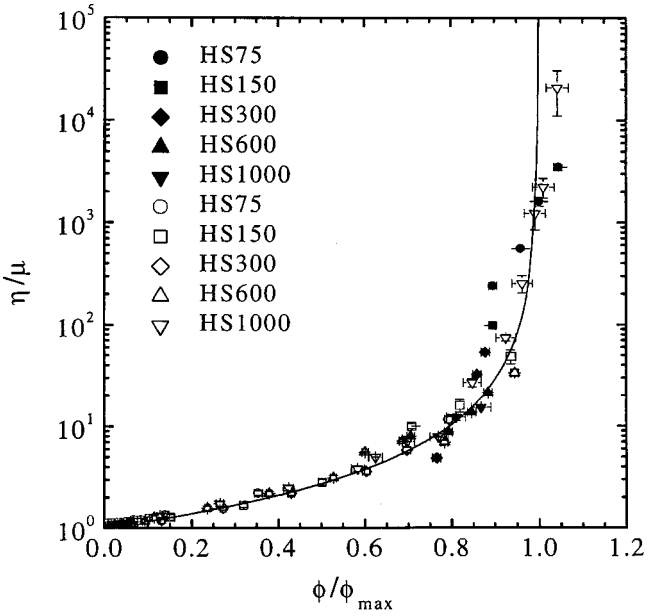

FIG. 4. Comparison of zero shear viscosity data between the HS75 dispersions with 0.066 M HNO_3 (filled symbols) and 0 M HNO_3 (open symbols) plotted against the volume fraction normalized by the maximum packing volume fraction. $\phi_{\max}$ values are listed in Table I. The line is the Krieger–Dougherty equation [Krieger and Dougherty (1959)].

As expected, the maximum packing fractions of the charge-neutralized dispersions are greater than those of the weakly charged dispersions because the added electrostatic repulsion increases the effective size of the latter dispersions. Wagner and co-workers (1991) have shown that the effective particle size of charged particles can be estimated as the hard-core radius plus a characteristic distance due to the electrostatic repulsion, which they take as a multiple of the Debye length. Maranzano and Wagner (2001) have demonstrated that this approach provides a reasonable estimate for the effective size of the original dispersions, and further that the increase in radius of the particle corresponds to where the electrostatic potential decays to $\approx 1\, k_B T$. However, since no measurable electrostatic interactions are present on the charge-neutralized dispersions, the small decrease in maximum packing relative to the hard-sphere value of 0.58 may be attributed to short range (i.e., $\sim$ nanometers) surface forces. These forces could arise from roughness or inhomogeneities in the TPM coating, or adsorbed water and ions from the acid used to neutralize the residual surface charge. Calculations for the necessary increase in radii, Δr (Table I) required to yield a maximum packing fraction of 0.58 show them to be comparable to or less than the breadth of the size distribution (a few percent of the particle size). Further, these derivatives in $\phi_{\max}$ may result from calculating the volume fraction directly from the measured particle densities as determined from high precision solution densitometry. Previous investigations have generally *fit* their volume fractions to obtain hard sphere intrinsic viscosities [de Kruif *et al.* (1985)] or to mimic the predicted phase behavior of hard spheres [Ackerson and Pusey (1988), Phan *et al.* (1996)]. Despite such adjustments, recent high-frequency modulus measurements on crystallized PMMA–PHSA systems exhibit deviations from expected hard sphere behavior [Phan *et al.* (1999)]. Consequently, to within the precision of our measurements and the paucidispersity of our particles, we cannot unequivocally determine the nature of such short-range forces, if any, that influence the zero shear viscosities.

Figures 5 and 6 compare flow curves for both dispersions at equal particle concentrations. Upon charge neutralization the low shear rheology changes qualitatively and a Newtonian low-shear plateau is evident in Fig. 5. This illustrates the extreme sensitivity of the low shear viscosity in concentrated dispersions to relatively weak, short-range electrostatic forces. The high shear rheology of the dispersions are also significantly altered by neutralization of the residual surface charge as illustrated in Figs. 5 and 6.

The shear thickening in both dispersions is observed to be reversible, with hysteresis evident only at low applied stresses and at the highest particle concentrations for the charge-neutralized dispersions. The small hysteresis in the charge-neutralized dispersions is attributed to weak attractive forces, possibly arising from van der Waals force and/or hydrophobic forces. The former are known to be present due to the slight turbidity in the samples. The samples are observed to recover to their presheared viscosity and exhibit very reproducible rheology. For clarity, Figs. 5 and 6 show only the viscosities measured from high to low shear stress.

Observe from Fig. 5 that the critical stress values are lower for the charge-neutralized dispersions ($\tau_c \approx 170$ Pa) than for the charged dispersions ($\tau_c \approx 750$ Pa). This is expected given that the magnitude of the electrostatic repulsive force acting between two particles at these concentrations is calculated to be approximately $7\, k_B T/a$, whereas the Brownian force is only about half of that ($|F_{\text{Brownian}}| \approx 3\, k_B T/a$) at the same concentrations. The reduction in the repulsive force upon neutralization decreases the shear stress required to generate hydroclusters and therefore, shear thickening is observed to

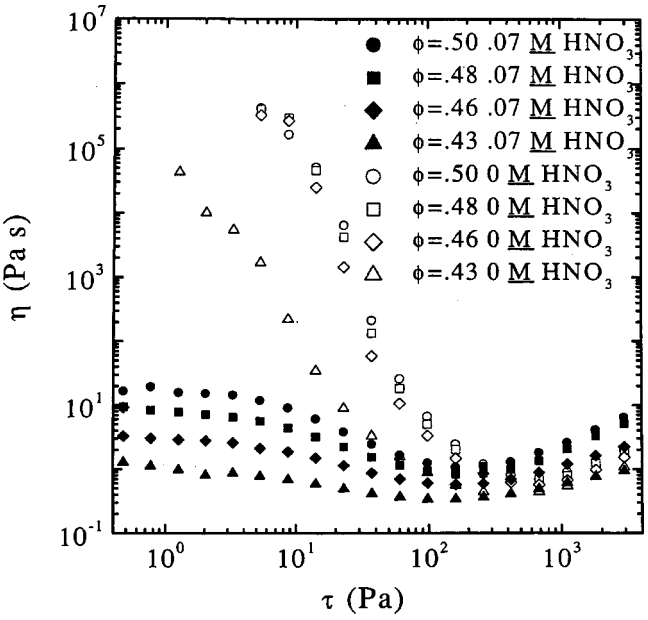

FIG. 5. Comparison of viscosity data between the HS75 dispersions with 0.066 M HNO_3 (filled symbols) and 0 M HNO_3 (open symbols) plotted against applied shear stress.

occur at lower stresses. This result is qualitatively in agreement with the simulation predictions of Melrose and co-workers [Melrose *et al.* (1996), Catherall *et al.* (2000)], who demonstrated that the addition of a conservative repulsive force (without any modification of the lubrication stresses) suppresses the onset of shear thickening.

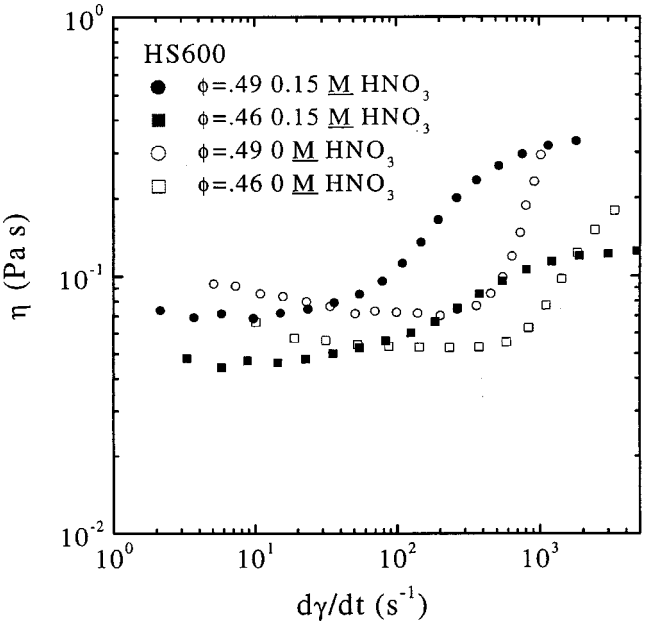

FIG. 6. Comparison of viscosity data between the HS600 dispersions with 0.066 M HNO_3 (filled symbols) and 0 M HNO_3 (open symbols) plotted against applied shear rate.

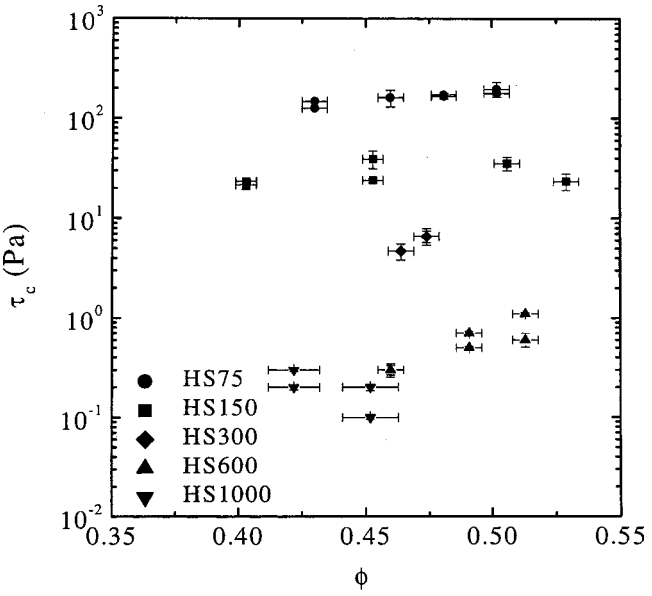

FIG. 7. Critical stress for shear thickening determined from a double logarithmic plot as a function of volume fraction for the various charge-neutralized dispersions.

There is a qualitative difference in the viscosity in the shear thickened state between the two types of dispersions. Figure 6 shows a plot of the viscosity plotted against shear rate for the charge-neutralized and original dispersions. Note that the viscosity for the original dispersions increases more sharply at the shear thickening transition, whereas the viscosity response of the charge-neutralized dispersions increases more gradually upon shear thickening. This behavior is consistent with the observation that lowering the volume fraction leads to a more gradual shear thickening transition; charge neutralization lowers the effective volume fraction, which quantitatively leads to the same behavior. Also observed that the viscosity of the charge-neutralized dispersions at shear stresses several magnitudes past the critical shear thickening stress begins to plateau, which may be due to extensive slip [Maranzano and Wagner (2001)].

The critical stresses for shear thickening are plotted for all of the charge-neutralized dispersions as a function of volume fraction in Fig. 7. The critical stress values span 3 decades and systematically increase with decreasing particle size, as is expected from the scaling Eq. (2). Also observe that the critical stress is relatively insensitive to the volume fraction, whereas a plot of the critical shear rate (not shown here) is not. This behavior is consistent with the mean-field approximation proposed by Bender and Wagner (1996) in deriving their scaling relation.

It has been shown by both simulation and experiment [Brady and Bossis (1988), D'Haene *et al.* (1993), Laun *et al.* (1992), Foss and Brady (2000), Bender and Wagner (1996), Melrose *et al.* (1996), OBrien and Mackay (2000), Maranzano and Wagner (2001), Newstein *et al.* (1999)] that shear thickening is a consequence of increased hydrodynamic interactions that accompany the formation of a correlated microstructure denoted as ''hydroclustered.'' The dominance of the lubrication hydrodynamic forces over stabilizing forces marks the onset of this microstructure formation. Simply considering the forces involved to be hydrodynamic and Brownian, and further estimating the values at the average surface-to-surface separation distance leads to the balance given in

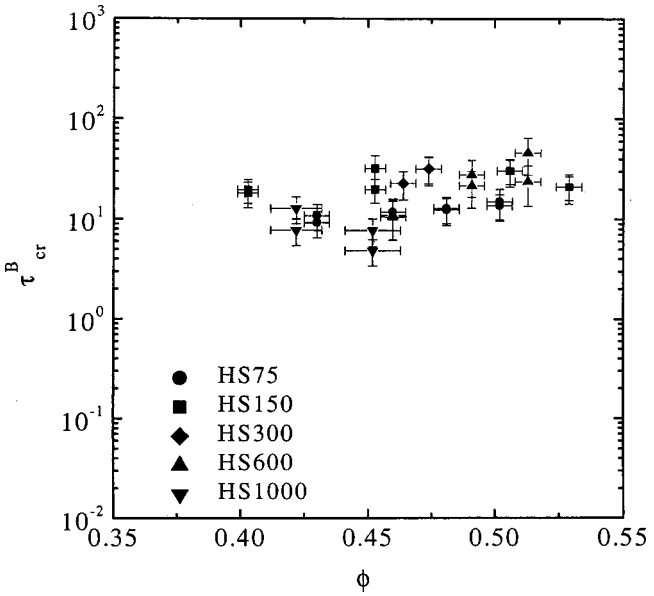

FIG. 8. Dimensionless critical stress for shear thickening proposed by Bender and Wagner as a function of volume fraction for the various charge-neutralized dispersions.

Eq. (2) above. The dimensionless critical stresses for all the charge-neutralized dispersions of varying particle size are plotted as a function of volume fraction in Fig. 8.

As seen by comparing Figs. 8 and 7, scaling the critical stress according to Eq. (2) collapses the data for dispersions of different particle sizes. There is no systematic variation in the reduced critical stress with particle size, demonstrating that the a^3 scaling is appropriate for Brownian dispersions. However, the average dimensionless stress (≈ 20) is not order one as expected, which may be a consequence of assuming the average separation distance between particles in calculating the Brownian force. A comparable plot for the electrostatically stabilized dispersions [see Fig. 13 in Maranzano and Wagner (2001)] failed to reduce the critical stresses.

A dimensionless critical stress plot using the modified Melrose and Ball (2000) model is not possible because the approximate criteria for the separation distance [Eq. (4)] cannot be satisfied. Instead, it is found that the compressive force at the onset of shear thickening is slightly larger than the maximum force obtainable solely from Brownian motion. This may be a consequence of the approximations underlying Eq. (4), or possibly, additional short range stabilizing forces that are not detected by electrophoretic mobility measurements or SANS. Nonetheless, the theory can be used *predictively* by solving simultaneously for both the stress required to balance the Brownian force in Eq. (4) and simultaneously, that required to satisfy the kinetic constraint [i.e., setting $\tau^M_{cr} = 1$ in Eq. (3)]. These predicted values are cross plotted against the measured values in Fig. 9. The correlation between the two data sets is good (0.993), but differs by a constraint proportionality of 1/2. This can easily be attributed to the neglect of order one constants in the scaling law. The results of the predictive model in addition to the a^{-3} scaling strongly supports the Brownian motion as the dominant repulsive force stabilizing the particles.

On the contrary, the original dispersions [Maranzano and Wagner (2001)] and other charge-stabilized dispersions [Boersma *et al.* (1990)] show an a^{-2} scaling that results

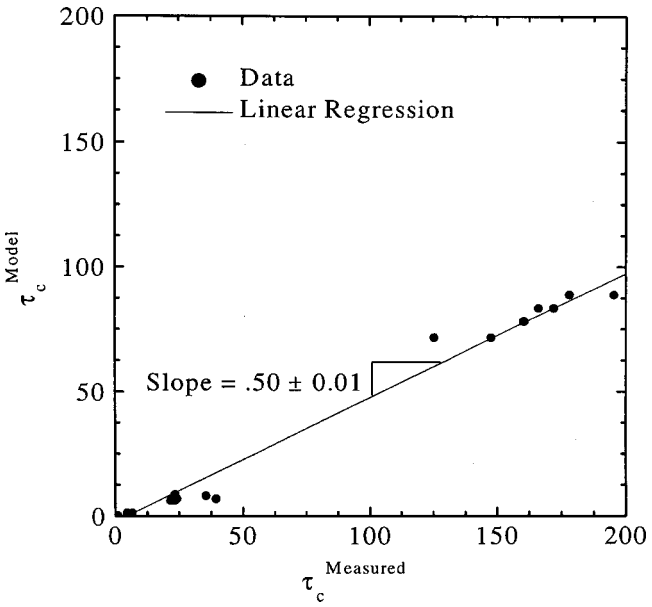

FIG. 9. The critical stress for shear thickening *predicted* from Eqs. (4) and (3) plotted against the measured critical stress for shear thickening for the charge-neutralized dispersions. The correlation coefficient between the two sets of data is 0.993.

when surface forces are the dominant stabilization mechanism. This is consistent with the fact that surface forces scale with the surface area, whereas Brownian forces scale with the particle volume. The consequence of this is that previous attempts to correlate shear thickening with particle size across wide variations in particle type have been less successful [Barnes (1989)].

Previous rheological measurements on model, hard-sphere dispersions by de Kruif and co-workers (1985) did not exhibit shear thickening over the range of shear rates and volume fractions investigated. Their systems are stabilized by grafted oligomers (octadecanol) and are dispersed in a good solvent for the coating (cyclohexane). However, Frith and co-workers (1996) observed shear thickening in systems with similar grafted layers in other solvents. To demonstrate the differences in de Kruif's rheology data with ours on the reversible shear thickening transition, Figs. 10 and 11 show two plots of our data using the procedure they employed to collapse their data. The characteristic stress, σ_c, used to nondimensionalize the applied shear stress and the high shear limiting viscosity (which could not be measured due to the shear thickening) is taken from their work, whereas our measured zero shear viscosity is used. The scaling does an acceptable job of collapsing the data in the shear thinning region, but the value of σ_c is too large by a factor of ~ 3 to bring our data in line with theirs. Comparison with their reported data shows that their measurements ended in the vicinity of the critical stress for shear thickening ($\tau_c/\sigma_c \sim 4$). Thus, it is not evident if their grafted octadecyl layer alters the shear thickening behavior, as would be expected from the predictions of Melrose and Ball [Melrose and Ball (2000)].

On the contrary, the PMMA–PHSA systems by Frith *et al.* (1996) do exhibit shear thickening similar to that observed here. Furthermore, as they collapse the swollen layer by changing solvent quality, their scaling for shear thickening changes from $\dot{\gamma}_c \propto a^{-2}$ to

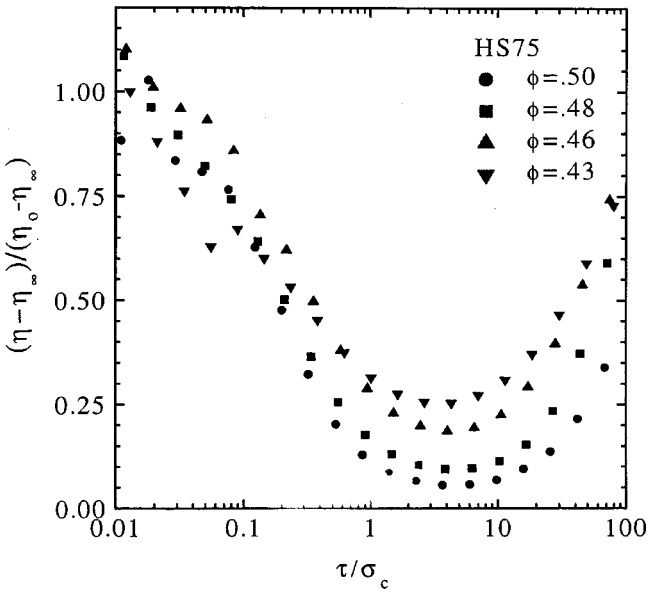

FIG. 10. Dimensionless viscosity plotted against stress scaled by the characteristic stress (σ_c) of de Kruif *et al.* for the HS75 dispersion.

$\dot{\gamma} \propto a^{-3}$. The a^{-2} scaling is expected when surface forces dominate, as shown by Boersma [Boersma *et al.* (1990)]. Thus, although the PMMA–PHSA system can be used to study hard-sphere phase behavior by suitable rescaling of the particle size to account for the swollen adsorbed polymer layer, the high shear rheological behavior is demon-

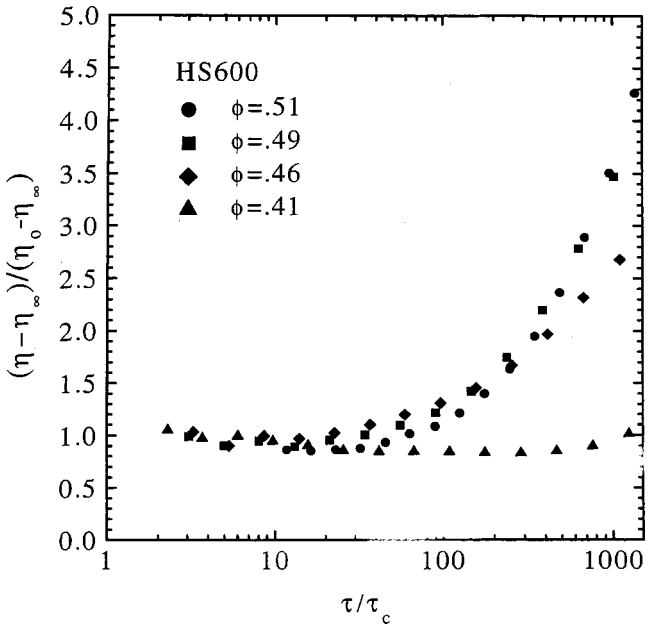

FIG. 11. Dimensionless viscosity plotted against stress scaled by the characteristic stress of de Kruif *et al.* for the HS600 dispersion.

strated to be very sensitive to the nature of the stabilizing layer. This is in qualitative agreement to the simulation results of Melrose *et al.* (1996).

V. CONCLUSIONS

The addition of a small amount of nitric acid ($c_{HNO_3} \approx 0.1$ M) to a dispersion of TPM coated silica in an index matched organic solvent (THFFA) is sufficient to suppress the electrophoretic mobility and lead to paucidisperse hard-sphere SANS spectra. The charge-neutralized dispersions exhibit rheology consistent with that predicted for hard spheres. Comparison between charge-neutralized and electrostatically stabilized dispersions qualitatively validates model predictions that additional, conservative forces act to suppress the onset of shear thickening in concentrated, stable dispersions. The critical stress for the onset of reversible shear thickening for the hard-sphere dispersions is shown to scale with the inverse particle size cubed, which is in agreement with predictions for hard spheres. Comparison to previous data in the literature for hard-sphere systems with larger, grafted stabilizers in good solvent suggest that the high shear rheology of colloidal dispersions is extremely sensitive to the detailed, short range forces acting between particles. This sensitivity is consistent with the formation of hydroclusters and the dominance of short-range lubrication forces in the shear thickened state. Finally, to within the accuracy of the approximations in the modeling, the data here support the simple, two-particle model for the onset of shear thickening as the incipient stress-induced formation of long-lived, correlated density fluctuations.

ACKNOWLEDGMENTS

This work was supported by the National Science Foundation (CTS-9523268) and the International Fine Particle Research Institute. This work benefitted from extensive discussions with J. F. Brady, J. R. Melrose, and J. Mewis, who are gratefully acknowledged. The SANS measurements were performed at the National Institute of Standards and Technology under Agreement No. NSF DMR-912244.

References

Ackerson, B. J. and P. N. Pusey, ''Shear-induced order in suspensions of hard spheres,'' Phys. Rev. Lett. **61**, 1033–1036 (1988).

Barnes, H. A., ''Shear-thickening (dilatancy) in suspensions of nonaggregating solid particles dispersed in newtonian fluids,'' J. Rheol. **33**, 329–366 (1989).

Batchelor, G. K., ''The stress systems in a suspension of force-free particles,'' J. Fluid Mech. **41**, 545–570 (1970).

Batchelor, G. K., ''The effect of brownian motion on the bulk stress in a suspension of spherical particles,'' J. Fluid Mech. **83**, 97–117 (1997).

Batchelor, G. K. and J. T. Green, ''The determination of the bulk stress in a suspension of spherical particles to order c^2,'' J. Fluid Mech. **56**, 401–472 (1972).

Bender, J. W. and N. J. Wagner, ''Optical measurement of the contributions of colloidal forces to the rheology of concentrated suspensions'' J. Colloid Interface Sci. **172**, 171–184 (1995).

Bender, J. W. and N. J. Wagner, ''Reversible shear thickening in monodisperse and bidisperse colloidal dispersions,'' J. Rheol. **40**, 899–916 (1996).

Boersma, W. H., J. Laven, and H. N. Stein, ''Shear thickening (dilatancy) in concentrated dispersions,'' AIChE J. **36**, 321–332 (1990).

Bossis, G. and J. F. Brady, ''The rheology of brownian suspensions,'' J. Chem. Phys. **91**, 1866–1874 (1989).

Brady, J. and J. Morris, ''Microstructure of strongly sheared suspensions and its impact on rheology and diffusion,'' J. Fluid Mech. **348**, 103–139 (1997).

Brady, J. F., ''The rheological behavior of concentrated colloidal dispersions,'' J. Chem. Phys. **99**, 567–581 (1993).
Brady, J. F. and G. Bossis, ''Stokesian dynamics,'' Annu. Rev. Fluid Mech. **20**, 111–157 (1988).
Catherall, A. A., J. R. Melrose, and R. C. Ball, ''Shear thickening and order-disorder effects in concentrated colloids at high shear rates,'' J. Rheol. **44**, 1–25 (2000).
Chow, M. K. and C. F. Zukoski, ''Gap size and shear history dependencies in shear thickening of a suspension ordered at rest,'' J. Rheol. **39**, 15–32 (1995).
de Kruif, C. G., E. M. F. van Iersel, A. Vrij, and W. B. Russel, ''Hard sphere colloidal dispersions: Viscosity as a function of shear rate and volume fraction,'' J. Chem. Phys. **83**, 4717–4725 (1985).
D'Haene, P., J. Mewis, and G. G. Fuller, ''Scattering dichroism measurements of flow-induced structure of a shear thickening suspension,'' J. Colloid Interface Sci. **156**, 350–358 (1993).
Dratler, D. I. and W. R. Schowater, ''Dynamic simulation of suspensions of non-brownian hard spheres,'' J. Fluid Mech. **325**, 53–77 (1996).
Farr, R. S., J. R. Melrose, and R. C. Ball, ''Kinetic theory of jamming in hard-sphere startup flows,'' Phys. Rev. E **55**, 7203–7211 (1997).
Foss, D. and J. Brady, ''Structure, diffusion and rheology of brownian suspensions by stokesian dynamics simulation,'' J. Fluid Mech. **407**, 167–200 (2000).
Frankel, N. A. and A. Acrivos, ''On the viscosity of a concentrated suspension of solid spheres,'' Chem. Eng. Sci. **22**, 847–853 (1967).
Frith, W. J., P. d'Haene, R. Buscall, and J. Mewis, ''Shear thickening in model suspensions of sterically stabilized particles,'' J. Rheol. **40**, 531–548 (1996).
Gast, A. P. and C. F. Zukoski, ''Electrorheological fluids as colloidal suspensions,'' Adv. Colloid Interface Sci. **30**, 153–202 (1989).
Griffith, W. L., R. Triolo, and A. L. Compere, ''Analytical scattering function of a polydisperse Percus-Yevick fluid with Schulz-(gamma) distributed diameters,'' Phys. Rev. A **35**, 2200–2206 (1987).
Hoffmann, R. L., ''Discontinuous and dilatant viscosity behavior in concentrated suspensions I. Observation of a flow instability,'' Trans. Soc. Rheol. **16**, 155–15 (1972).
Iler, R. K., *The Colloid Chemistry of Silica and Silicates* (Cornell University Press, Ithaca, NY, 1955).
Jeffrey, D. J. and A. Acrivos, ''The rheological properties of suspensions of rigid particles,'' AIChE J. **22**, 417–430 (1976).
Kaffashi, B., V. T. OBrien, M. E. Mackay, and S. M. Underwood, ''Elastic-like and viscous-like components of the shear viscosity for nearly hard sphere,'' J. Colloid Interface Sci. **181**, 22–28 (1997).
Krieger, I. M. and T. J. Dougherty, ''A mechanism for non-newtonian flow in suspensions of rigid spheres,'' Trans. Soc. Rheol. **3**, 137 (1959).
Laun, H. M. *et al.*, ''Rheological and small angle neutron scattering investigation of shear-induced particle structures of concentrated polymer dispersions submitted to plane poiseuille and coutte flow,'' J. Rheol. **36**, 743–787 (1992).
Lionberger, R. and W. Russel, ''A smoluchowski theory with simple approximations for hydrodynamic interactions in concentrated dispersions,'' J. Rheol. **41**, 399–425 (1997).
Maranzano, B. J. and N. J. Wagner, ''The effects of particle size on reversible shear thickening of concentrated colloidal dispersions,'' J. Chem. Phys. **114**, 10514–10527 (2001).
Maranzano, B. J., ''Rheology and microstructure of near hard sphere colloidal dispersions at the shear thickening transition,'' Ph.D. thesis, University of Delaware, 2001.
Maranzano, B. J., N. J. Wagner, G. Fritz, and O. Glatter, ''Surface charge and microstructure of 3-(trimethoxysilyl) propyl methacrylate (tpm) coated stöber silica colloids by zeta-PALS and SANS,'' Langmuir **16**, 10556–10558 (2000).
Meeker, S. P., W. C. K. Poon, and P. N. Pusey, ''Concentration dependence of the low-shear viscosity of suspensions of hard-sphere colloids,'' Phys. Rev. E **55**, 5718–5722 (1997).
Melrose, J. R. and R. C. Ball, ''The pathological behaviour of sheared hard spheres with hydrodynamic interactions,'' Europhys. Lett. **32**, 535–540 (1995).
Melrose, J. R. and R. C. Ball, ''A simulation technique for many spheres in quasi-static motion under frame-invariant pair drag and brownian forces,'' Physica A **247**, 444–472 (1997).
Melrose, J. R. and R. C. Ball, ''The granular physics of sheared thickened colloids,'' *XIIIth International Congress of Rheology*, 2000, Vol. 2, pp. 421–423.
Melrose, J. R., J. van Vliet, and R. C. Ball, ''Continuous shear thickening and colloid surfaces,'' Phys. Rev. Lett. **77**, 4660–4663 (1996).
Newstein, M. C., H. Wang, N. P. Balsara, A. A. Lefebvre, Y. Shnidman, H. Watanabe, K. Osaki, T. Shikata, H. Niwa, and Y. Morishima, ''Microstructural changes in a colloidal liquid in the shear thinning and shear thickening regimes,'' J. Chem. Phys. **111**, 4827–4838 (1999).
OBrien, V. T. and M. E. Mackay, ''Stress components and shear thickening of concentrated hard sphere suspensions,'' Langmuir **16**, 7931–7938 (2000).

Phan, S., M. Li, W. B. Russel, J. Zhu, P. M. Chaikin, and C. T. Lant, ''Linear viscoelasticity of hard sphere colloidal crystals from resonance detected with dynamic light scattering,'' Phys. Rev. E **60**, 1988–1998 (1999).

Phan, S. E., W. B. Russel, Z. D. Cheng, J. X. Chaikin, J. H. Dunsmuir, and R. H. Ottelwill, ''Phase transition, equation of state, and limiting shear viscosities of hard sphere dispersions,'' Phys. Rev. E **54**, 6633–6645 (1996).

Philipse, A. P. and A. Vrij, ''Preparation and properties of nonaqueous model dispersions of chemically modified charged silica spheres,'' J. Colloid Interface Sci. **128**, 121–136 (1998).

Rueb, C. J. and C. F. Zukoski, ''Rheology of suspensions of weakly attractive particles: Approach to gelation,'' J. Rheol. **42**, 1451–1476 (1998).

Russel, W. B. and A. P. Gast, ''Nonequilibrium statistical-mechanics of concentrated colloidal dispersions—hard-spheres in weak flows,'' J. Chem. Phys. **84**, 1815–1826 (1986).

Segre, P. N. and P. N. Pusey, ''Dynamics and scaling in hard-sphere colloidal suspensions,'' Physica A **235**, 9–18 (1997).

van Blaaderen, A. and A. Vrij, ''Synthesis and characterization of monodisperse colloidal organo-silica spheres,'' J. Colloid Interface Sci. **156**, 1–18 (1993).

van der Werff, J. C. and C. G. de Kruif, ''The scaling of rheological properties with particle size, volume fraction and shear rate,'' J. Rheol. **33**, 421–454 (1989).

van der Werff, J. C., C. G. de Kruif, and J. K. G. Dhont, ''The shear-thinning behaviour of colloidal dispersions 1. Some theoretical considerations,'' Physica A **160**, 195–204 (1989).

Wagner, N. J., G. Fuller, and W. B. Russel, ''The dichroism and birefringence of a hard-sphere suspension under shear,'' J. Chem. Phys. **89**, 1580–1587 (1988).

Wagner, N. J., R. Krause, A. R. Rennie, B. D'Aguanno, and J. Goodwin, ''The microstructure of polydisperse, charged colloidal suspensions by light and neutron scattering,'' J. Chem. Phys. **95**, 494–508 (1991).

Wagner, N. J. and W. B. Russel, ''Nonequilibrium statistical-mechanics of concentrated colloidal dispersions—hard-spheres in weak flows with many-body thermodynamic interactions, Physica A **155**, 475–518 (1989).

Wagner, N. J. and W. B. Russel, ''Light-scattering measurements of a hard-sphere suspension under shear,'' Phys. Fluids A **2**, 491–502 (1990).

Wilson, H. J. and R. H. Davis, ''The viscosity of a dilute suspension of rough spheres,'' J. Fluid Mech. **421**, 339–367 (2000).